Energy and momentum broadening of planar microcavity polaritons measured by resonant light scattering

2004 J. Phys.: Condens. Matter 16 S3645

(http://iopscience.iop.org/0953-8984/16/35/006)

INSTITUTE OF PHYSICS PUBLISHING JOURNAL OF PHYSICS: CONDENSED MATTER

J. Phys.: Condens. Matter **16** (2004) S3645–S3652 PII: S0953-8984(04)83318-6

Energy and momentum broadening of planar microcavity polaritons measured by resonant light scattering

Wolfgang Langbein

Experimentelle Physik IIb, Universität Dortmund, Otto-Hahn Straße 4, 44227 Dortmund, Germany

Received 6 July 2004
Published 20 August 2004
Online at stacks.iop.org/JPhysCM/16/S3645
doi:10.1088/0953-8984/16/35/006

Abstract

We present measurements of polariton broadening in energy and momentum space as a function of in-plane momentum in a planar microcavity by directional resonant light scattering in both time-integrated and time-resolved experiments. When optically exciting the lower polariton branch, the strong dispersion versus wavevector results in a directional emission on a ring. For continuous wave excitation, the ring width is shown to be consistent with the polariton spectral line width and dispersion. For pulsed excitation, the ring width decreases with increasing time after excitation, giving evidence for the time–energy uncertainty in the dynamics of the scattering by disorder. The ring width converges for long times to a finite value, a measure of the intrinsic momentum broadening of the polariton states by multiple disorder scattering.

1. Introduction

In resonant secondary emission (SE) of light, scattering by static disorder leads to coherent resonant Rayleigh scattering (RRS), while scattering by other quasi-particles (e.g. phonons) leads to incoherent emission. In planar semiconductor microcavities (MCs), cavity polaritons are formed [1] with a strong dispersion at small in-plane wavevectors $\mathbf{k}$. In this case, the energy conservation in the RRS translates into directional RRS. Accordingly, annular RRS has been predicted [2, 3] and enhanced RRS on a ring was found experimentally [4, 5]. The dynamics of the RRS was shown to be governed by the energy–time uncertainty in the disorder scattering [6].

In this work, we investigate directional RRS from the lower polariton (LP) branch of a MC both for resonant continuous wave (cw) and pulsed excitation of the LP. In the cw measurements the width of the RRS ring in the radial direction, i.e. in $k = |\mathbf{k}|$, is found to be in agreement with the measured LP spectral line width and the LP dispersion. For pulsed excitation, the RRS ring width decreases with time according to energy–time uncertainty in

Table 1. Parameters of the three-coupled-oscillator model used in the presented calculations.

Name	Value	Unit
Heavy-hole exciton energy, $E^0_{\rm hh}$	1.521 60	eV
Light-hole exciton energy, $E^0_{\rm lh}$	1.524 15	eV
Heavy-hole exciton in-plane mass, $M_{\rm hh}$	0.4	$m_{\rm e}$
Light-hole exciton in-plane mass, $M_{\rm lh}$	0.4	$m_{\rm e}$
Heavy-hole exciton Rabi energy, $2\Omega_{\rm hh}$	3.65	meV
Light-hole exciton Rabi energy, $2\Omega_{\rm hh}$	2.2	meV
Cavity effective refractive index, $n_{\rm eff}$	3.5	—

the disorder scattering, down to a minimum width that is given by the k broadening of the polariton eigenstates.

2. Investigated sample and experiment

The investigated sample [7] consists of an MBE-grown 25 nm $GaAs/Al_{0.3}Ga_{0.7}As$ single quantum well (QW) placed in the centre of a λ-cavity with $AlAs/Al_{0.15}Ga_{0.85}As$ Bragg reflectors of 25 (16) periods at the bottom (top). The sample was held in a helium cryostat at a temperature of $T = 5$ K. The cw excitation was provided by a tunable diode laser of a spectral line width below 10 μeV. The pulsed excitation was by Fourier-limited optical pulses from a mode-locked Ti:sapphire laser of 1 ps pulse duration at 76 MHz repetition rate. The excitation was focused on the sample to a diffraction-limited spot of 100 μm diameter and a $\mathbf{k}$ width of 0.035 μm^{-1} in both in-plane directions. The excitation intensity was chosen low enough to be in a linear response regime. Spectrally resolved data were taken using a spectrometer with a resolution of 20 μeV. Time-resolved data were taken using a streak-camera with a resolution of 3 ps. The sample was characterized previously by reflection measurements [7, 8]. The use of a wide GaAs QW leads to a negligible inhomogeneous broadening of the QW exciton due to the small effect of interface roughness and the absence of alloy disorder in the well. The exciton–photon coupling in the MC creates three polariton resonances from the heavy-hole exciton, light-hole exciton and cavity mode. The polariton formation is quantitatively described by a three-coupled-oscillator model [7], which is presented in the appendix. From the measured polariton line widths a cavity line width of $\gamma_{\rm c} = 0.13$ meV HWHM and an excitonic line width of $\gamma_{\rm hh} = \gamma_{\rm lh} = 0.06$ meV HWHM were inferred [8]. We define the detuning of the MC as the energy difference between the cavity mode and heavy-hole exciton, which is negative if the cavity mode is at lower energy.

3. Excitation with defined frequency and wavevector

To characterize the LP dispersion $E_{\rm LP}(k)$, we measured the SE along $\mathbf{k} = (0, k_y)$, cross-polarized to the excitation, while the LP was excited resonantly with linearly polarized cw light at $\mathbf{k}_{\rm e} \approx (3.5, 0)\ \mu m^{-1}$. Experimental results are given in figure 1 for different detunings. The strong resonant emission at the excitation energy, and the non-resonant emission from the LP and the middle polariton are observed. The dispersion is compared with the results of the three-coupled-oscillator model (dotted curves) using the parameters given in table 1 and a good quantitative agreement with the model is found.

For co-linear detection, the resonant emission is dominated by elastic scattering. The resulting emission intensity in $\mathbf{k}$-space is shown in figure 2 for a detuning of -6 meV and

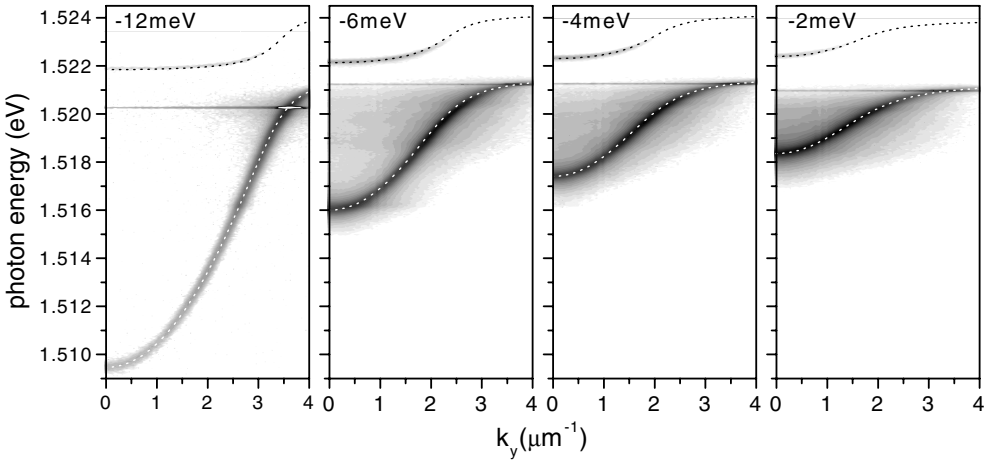

Figure 1. Wavevector-resolved secondary emission spectra of the MC for $\mathbf{k} = (0, k_y)$, cross-linearly polarized to the resonant cw excitation of the LP at $\mathbf{k}_e = (3.5, 0)$. Logarithmic grey-scale covering three orders of magnitude increasing from white to black. The dotted curves are calculations within a three-coupled-oscillator model (see the appendix). Data for different detunings, as indicated, are shown.

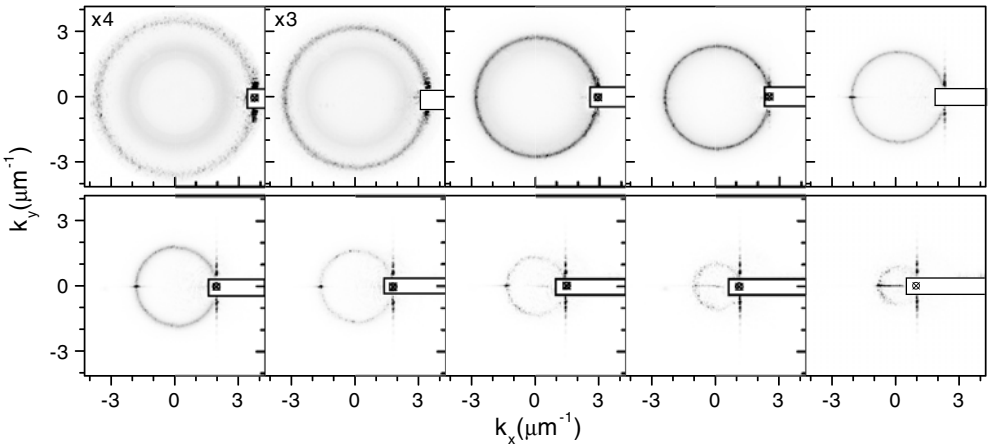

Figure 2. Secondary emission intensity $\mathbf{k}$ images, co-linearly polarized to the resonant cw excitation of the LP. Data for −6 meV detuning. Linear grey-scale from white to black. The crosses indicate $\mathbf{k}_e$, and the rectangles are blocks of the specular (primary) emission.

different k_e. The specular emission, indicated by a cross, is blocked within the white rectangular regions. For the largest k_e, the emission consists of a coherent RRS ring at $k = k_e$, and photoluminescence of bound excitons (BE) at lower energy via the polariton states at smaller k. The RRS ring shows strong fluctuations on a small directional scale, i.e. speckles, which demonstrate its dominant coherent nature. With decreasing k_e, the RRS ring narrows. For resonant excitation of the BE energy region ($k_e \approx 2$–$3\ \mu\text{m}^{-1}$), photoluminescence of the BE also contributes to the ring, as is visible by the reduced speckle contrast and the increased intensity on the ring. With further decreasing k_e, the BE emission vanishes, and an additional cross-shaped scattering along the k_x and k_y directions, coinciding with the [110] and [1$\bar{1}$0]

in-plane crystallographic directions of the sample, becomes increasingly important. The well defined scattering directions imply a correlation length of the underlying disorder comparable to the spot size. Its origin is the cross-hatched disorder forming in lattice-mismatched growth [9] due to interfacial misfit dislocations. It forms in the AlAs Bragg-mirrors, which have 0.2% lattice mismatch to GaAs, and a thickness of several micrometres. Corresponding stripes are observed in surface images of the RRS (not shown). The importance of this disorder type for small k_e, for which the photonic content is large (50–88%), and its absence for large k_e, for which the photonic content is small (5–10%), shows that it acts dominantly on the cavity mode. We therefore speculate that it is present in the top Bragg mirror only, and that the corresponding dislocations do not penetrate through the QW.

We now focus on the RRS ring, which shows a nearly azimuthally isotropic intensity distribution. We conclude from this that the underlying disorder has a correlation length shorter than the light wavelength. As we have seen in the behaviour of the stripe-like scattering, the disorder acting on the excitonic and the photonic part of the polariton is different. This is expected since the excitonic part is sensitive to the disorder in the QW only, while the photonic part extends into the Bragg mirrors. Also the way interface roughness and strain disorder affect the photonic and excitonic parts is different, but a detailed discussion of this point is beyond the scope of this work. We assume that the disorder potentials $V_{\mathrm{hh,lh,c}}$ acting on the respective parts of the polariton are of short correlation length and are mutually uncorrelated, with disorder averages $\langle V_{\mathrm{hh}}^2\rangle$, $\langle V_{\mathrm{lh}}^2\rangle$, and $\langle V_{\mathrm{c}}^2\rangle$ for the heavy-hole exciton, the light-hole exciton and the cavity mode, respectively. The disorder averaged scattering intensity $I_{\mathrm{RRS}}(k)$ for an excitation of intensity I_{e}, wavevector $\mathbf{k}_{\mathrm{e}}$ and energy E_{e} is then in a single scattering approximation expected to be

$$I_{\mathrm{RRS}}(k) \propto I_{\mathrm{e}} c(k_{\mathrm{e}}) c(k) \frac{x_{\mathrm{hh}}(k) x_{\mathrm{hh}}(k_{\mathrm{e}}) \langle V_{\mathrm{hh}}^2\rangle + x_{\mathrm{lh}}(k) x_{\mathrm{lh}}(k_{\mathrm{e}}) \langle V_{\mathrm{lh}}^2\rangle + c(k) c(k_{\mathrm{e}}) \langle V_{\mathrm{c}}^2\rangle}{|E_{\mathrm{e}} - E_{\mathrm{LP}}(k_{\mathrm{e}}) - \mathrm{i}\gamma_{\mathrm{LP}}(k_{\mathrm{e}})|^2 |E_{\mathrm{e}} - E_{\mathrm{LP}}(k) - \mathrm{i}\gamma_{\mathrm{LP}}(k)|^2}. \tag{1}$$

For maximum scattering efficiency, the incoming energy resonance condition $E_{\mathrm{e}} = E_{\mathrm{LP}}(k_{\mathrm{e}})$ was adjusted for all measurements. The cavity and exciton contents c, x_{hh}, x_{lh} of the outgoing polaritons only slowly vary with k, so that the ring width in k is mainly determined by the outgoing energy resonance. Developing at the resonance point $k = k_{\mathrm{e}}$, we find

$$I_{\mathrm{RRS}}(k) \propto \frac{1}{\gamma_{\mathrm{LP}}^2(k_{\mathrm{e}}) \left[(k - k_{\mathrm{e}})^2 (\partial_k E_{\mathrm{LP}}(k_{\mathrm{e}}))^2 + \gamma_{\mathrm{LP}}^2(k_{\mathrm{e}})\right]}, \tag{2}$$

a Lorentzian of a FWHM of $2\gamma_{\mathrm{LP}}(k_{\mathrm{e}})/\partial_k E_{\mathrm{LP}}(k_{\mathrm{e}})$. We use this result to compare it with the measured width of the RRS ring. The experimental RRS ring width is determined by calculating the azimuthal average of $I_{\mathrm{RRS}}(\mathbf{k})$, excluding the stripe-like scattering, and fitting it by a Lorentzian. The resulting FWHM and centre positions are shown as squares in figure 3 for different excitation energies and detunings. The experimental results are compared with the prediction of equation (2). Therein we use the dispersion and spectral line width either determined from equation (6) of the three-oscillator model (solid curves), or determined by the measured k-resolved photoluminescence (dotted curves). Generally, a good quantitative agreement between the experimental results and the predictions is found. Deviations in the region of the BE emission from the predictions using the three-coupled-oscillator model can be attributed to an additional polariton line width by the resonant absorption into the BE. These deviations are not present in the comparison with the prediction using the experimental line widths.

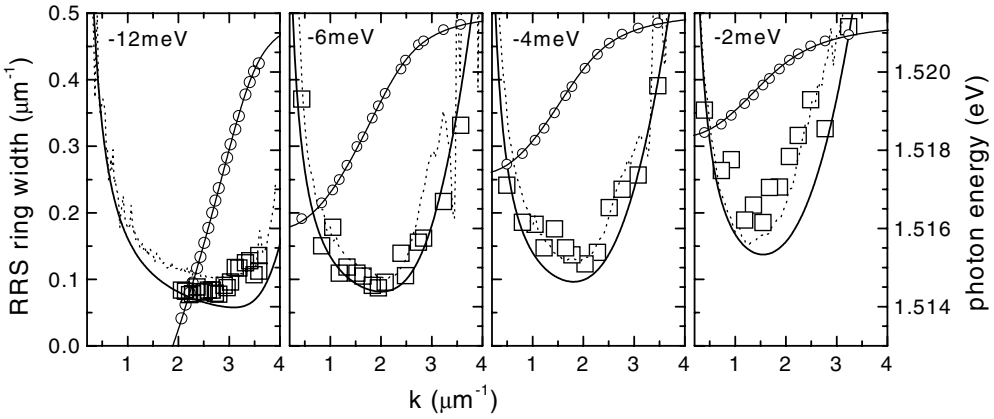

Figure 3. Width of the RRS ring in k as a function of the ring radius k. Measurements (squares) are compared with the values expected from the polariton spectral line width (dotted and thick curves, see text). The resonant excitation energies are shown as circles and are compared with the calculated polariton dispersion (thin curves). Data are shown for different detunings, as labelled.

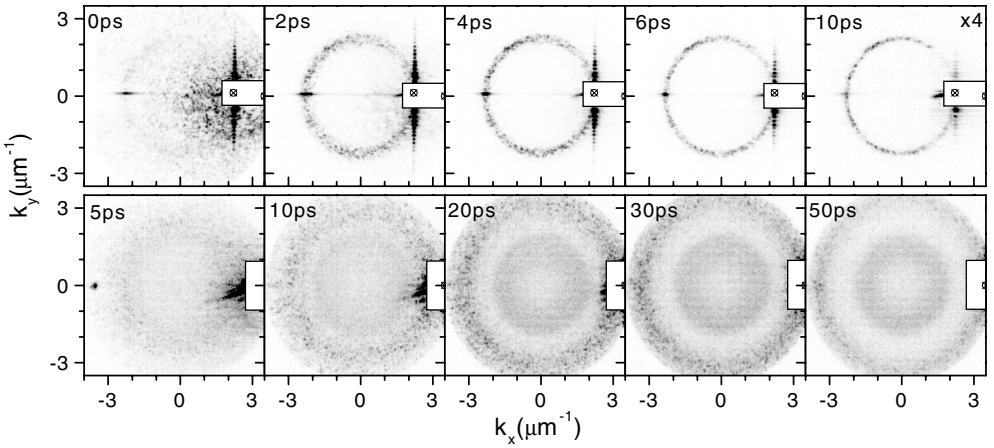

Figure 4. Secondary emission intensity **k** images, co-linearly polarized to the excitation, for different times after resonant pulsed excitation of the LP as labelled. Data are shown on a linear grey-scale from white (zero) to black (fixed positive value for each row, unless indicated). The crosses represent $\mathbf{k}_e$, and the rectangles are blocking the primary emission. Top: data for -12 meV detuning and $\mathbf{k}_e = (2.2, 0)\ \mu\text{m}^{-1}$. Bottom: data for -2 meV detuning and $\mathbf{k}_e = (3.2, 0)\ \mu\text{m}^{-1}$.

4. Excitation with defined time and wavevector

In this section we discuss the time-resolved emission for pulsed excitation. Under these conditions, polaritons are excited impulsively at $\mathbf{k}_e$ and $t = 0$, and scatter subsequently by the disorder present in the MC. Such dynamics has been discussed in [6], and we present here an extended study. We measured the two-dimensional dynamics of the polariton density by combining multiple streak-camera measurements of linear slices in **k**-space. In figure 4 the resulting **k**-images of the emission intensity, which is proportional to the polariton density times the photonic content, are shown for different times after the excitation. The specular emission, which is 4–5 orders of magnitude more intense than the RRS, is blocked from the

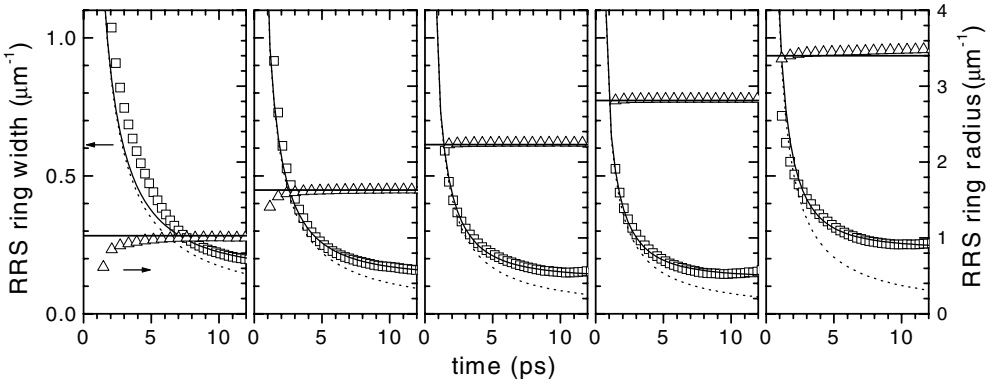

Figure 5. Time-dynamics of the position (triangles) and the width (squares) of the RRS ring in the radial direction. Data are shown for a detuning of −12 meV and different $\mathbf{k}_e$ which are indicated by the horizontal lines. The width dynamics is compared with the prediction of equation (3) using $\Delta k_{LP} = 0$ (dotted curves), and a fitted Δk_{LP} (solid curves), with values as displayed in figure 6.

detection. In the time-resolved experiments, stripe-like scattering along the [110] and [1$\bar{1}$0] directions also occurs, which is strong for a large cavity content (top row of figure 4), and essentially absent for a small cavity content (bottom row). The final states of this scattering are mainly non-resonant, i.e. not on the ring $|\mathbf{k}| = k_e$, so that the emission dynamics is mainly determined by the dynamics of the directly excited polaritons at $\mathbf{k}_e$. Consequently, it is faster than the dynamics on the RRS ring where the increasing transfer from $\mathbf{k}_e$ to the resonant final states on the ring is initially dominating over the radiative decay of the polariton density.

In the following we concentrate on the RRS ring. It can be observed that initially the RRS ring is rather broad in k, and narrows considerably with increasing time. The disorder leading to the RRS ring does not depend significantly on the scattering wavevector, as discussed earlier. The differences of the scattered polariton polarization $P(\mathbf{k})$ amplitudes are thus determined by the different mismatch of the polariton eigenenergies, i.e. $E_{LP}(k) - E_{LP}(k_e)$. The energy of the initially excited polarization $P(\mathbf{k}_e)$ is defined by its time-evolution. Its energy broadening is given therefore by the exciting pulse spectrum at $t \approx 0$, and narrows with time according to the time–energy uncertainty. The polarization can thus initially be scattered from $\mathbf{k}_e$ to a large k range. With increasing time, this k range decreases. The smaller the energy mismatch between $P(\mathbf{k}_e)$ and $P(\mathbf{k})$, the longer the scattering time between them, allowing for larger amplitudes to be transferred. This is an extreme case of non-Markovian behaviour due to the principally infinite memory time of scattering by static disorder [10]. The energy uncertainty of the $P(\mathbf{k}_e)$ polarization can be modelled using the time-bandwidth product $\Delta E \Delta t \approx 0.88$ h of a square time-window Δt where ΔE is the width of the energy distribution. The time window is the time between excitation of $P_{\mathbf{k}_e}$ and detection. From the energy width, the ring width is calculated using the measured dispersion $\partial_k E_{LP}$. This model, given by equation (3) with $\Delta k_{LP} = 0$ (see dotted curves in figure 5), reproduces the measured ring width dynamics for early times only, while for larger times the experimental width is underestimated. The experimental resolution, given by the $\mathbf{k}$ width of the excitation (0.035 μm^{-1}), cannot account for this deviation. We conclude that the polariton eigenstates are not pure $\mathbf{k}$ eigenstates, but are broadened in $\mathbf{k}$-space. For long times, the width of the ring thus converges not to zero, but to the finite $\mathbf{k}$ width of the excited polariton eigenstates. The $\mathbf{k}$ broadening of the polariton eigenstates is relevant both in their excitation by the external light pulse, and in the re-emission of the RRS. In the modelling we include the $\mathbf{k}$ broadening of the polariton eigenstates by adding an intrinsic polariton k

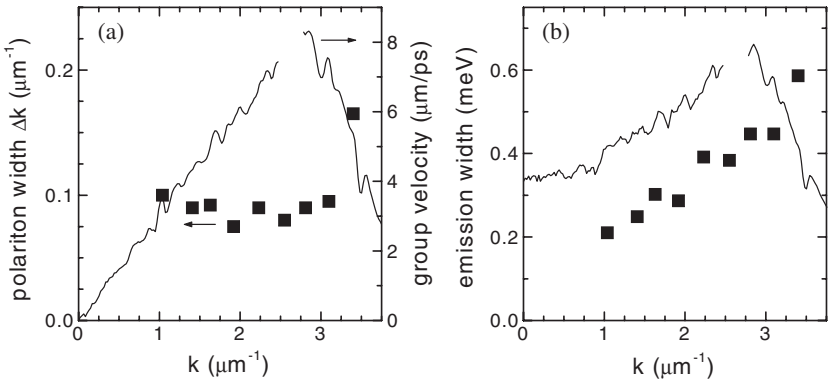

Figure 6. (a) Intrinsic polariton k width Δk_{LP} (squares) determined from the fit of equation (3) to the experimental RRS ring width dynamics at a detuning of -12 meV as a function of the average in-plane wavevector k. The polariton group velocity $\hbar^{-1}\partial_k E_{\mathrm{LP}}$, deduced from the measured $E_{\mathrm{LP}}(k)$ in photoluminescence is shown for comparison (curve). (b) Energy width $\Delta k_{\mathrm{LP}}\partial_k E_{\mathrm{LP}}$ (squares), compared with the emission linewidth in photoluminescence.

width Δk_{LP} in excitation and in emission in a Gaussian sum. The time-resolved width of the RRS is then described by:

$$\Delta k(\Delta t) = \sqrt{\left(\frac{0.88h}{\Delta t}\partial_k E_{\mathrm{LP}}\right)^2 + 2\Delta k_{\mathrm{LP}}^2}. \tag{3}$$

The experimental data are in good agreement with this model when using Δk_{LP} as a fit parameter (solid curves in figure 5).

The resulting values of Δk_{LP} are displayed in figure 6(a). They give a lower limit for the spatial extent of the polariton eigenstates. A rather constant value of Δk_{LP} versus k is found, despite the strongly varying group velocity (curve) of the related polaritons. The corresponding inhomogeneous emission line width $\Delta k_{\mathrm{LP}}\partial_k E_{\mathrm{LP}}$ is compared in figure 6(b) with the measured emission linewidth in photoluminescence. This comparison suggests that the observed increase of the emission linewidth with k is due to an inhomogeneous broadening of the polariton states emitting into a specific k.

The analysis of the emission at smaller detunings is complicated by the strong resonant emission of BE states spectrally overlapping with the RRS. In principle, speckle analysis [11] could be used to separate the coherent part of the emission from the incoherent one. However, the available data did not contain a sufficiently large speckle ensemble. For small detunings and large k_{e}, the polariton energy can be in the small energy range between the BE and the free exciton energy of less than 1 meV width, so that no BE emission overlaps with the RRS ring. Such a case is shown in the lower row of figure 4. The photonic content and the dispersion under these conditions are small, and the polariton decay dynamics is slow due to the small cavity content. In the specific case shown, the photonic content is 5%, and the dispersion is 0.32 meV μm. Also, here, equation (3) describes the dynamics of the ring width, yielding $\Delta k_{\mathrm{LP}} = 0.45\,\mu\mathrm{m}^{-1}$. The polaritons at large k have thus a large k-broadening, as expected by the small dispersion.

Acknowledgments

The sample was grown by J Riis Jensen at the Research Center COM and the Niels Bohr Institute, Copenhagen University. Continuous support by U Woggon is gratefully

acknowledged. This work was in part supported by the European Community's Human Potential Programme under contract HPRN-CT-2002-00298.

Appendix. Three coupled oscillator model including in-plane dispersion

We use the following energies of heavy-hole and light-hole excitons and cavity mode including their in-plane dispersion (symbols are explained in table 1):

$$E_{\mathrm{hh,lh}}(k) = E^0_{\mathrm{hh,lh}} + \frac{\hbar^2 k^2}{2M_{\mathrm{hh,lh}}}, \qquad E_{\mathrm{c}}(k) = E^0_{\mathrm{c}}\sqrt{1+\left(\frac{\hbar c k}{n_{\mathrm{eff}}E^0_{\mathrm{c}}}\right)^2}. \tag{4}$$

The coupling between the excitons and the cavity mode is described by the Rabi energies $\Omega_{\mathrm{hh,lh}}$, and the resulting polariton modes are given by the three eigenvectors $(X_{\mathrm{hh}}(\mathbf{k}), X_{\mathrm{lh}}(\mathbf{k}), C(\mathbf{k}))_{\mathrm{LP,MP,UP}}$ of the matrix

$$\begin{pmatrix} E_{\mathrm{hh}}(k) & 0 & \Omega_{\mathrm{hh}} \\ 0 & E_{\mathrm{lh}}(k) & \Omega_{\mathrm{lh}} \\ \Omega_{\mathrm{hh}} & \Omega_{\mathrm{lh}} & E_{\mathrm{cav}}(k) \end{pmatrix}, \tag{5}$$

with the eigenenergies $E_{\mathrm{LP}}(k) < E_{\mathrm{MP}}(k) < E_{\mathrm{UP}}(k)$. The index abbreviates the lower, middle and upper polariton branch. In the line width averaging model the exciton and cavity mode line width is introduced as an imaginary part $\gamma_{\mathrm{hh,lh,c}}$ of the eigenenergies. For small line widths compared to the Rabi energies, the eigenvectors can be assumed to be unchanged as well as the real part of the eigenenergies. The imaginary parts of the eigenenergies, which represent the polariton line widths, are then given by:

$$\gamma(k) = x_{\mathrm{hh}}(k)\gamma_{\mathrm{hh}} + x_{\mathrm{lh}}(k)\gamma_{\mathrm{lh}} + c(k)\gamma_{\mathrm{c}}, \tag{6}$$

with the excitonic contents $x_{\mathrm{hh,lh}}(k) = |X_{\mathrm{hh,lh}}(k)|^2$ and the cavity content $c(k) = |C(k)|^2$.

References

[1] Weisbuch C, Nishioka M, Ishikawa A and Arakawa Y 1992 *Phys. Rev. Lett.* **69** 3314
[2] Whittaker D M 2000 *Phys. Rev.* B **61** R2433
[3] Shchegrov A V, Bloch J, Birkedal D and Shah J 2000 *Phys. Rev. Lett.* **84** 3478
[4] Freixanet T, Sermage B, Bloch J, Marzin J Y and Planel R 1999 *Phys. Rev.* B **60** R8509
[5] Houdré R, Weisbuch C, Stanley R P, Oesterle U and Ilegems M 2000 *Phys. Rev.* B **61** R13333
[6] Langbein W and Hvam J M 2002 *Phys. Rev. Lett.* **88** 047401
[7] Jensen J R, Borri P, Langbein W and Hvam J M 2000 *Appl. Phys. Lett.* **76** 3262
[8] Borri P, Jensen J R, Langbein W and Hvam J M 2000 *Phys. Rev.* B **61** 13377
[9] Chang K H, Gilbala R, Srolovitz D J, Bhattacharya P K and Mansfield J F 1990 *J. Appl. Phys.* **67** 4093
[10] Zimmermann R 1995 *Nuovo Cimento* D **17** 1801
[11] Langbein W, Hvam J M and Zimmermann R 1999 *Phys. Rev. Lett.* **82** 1040